Energy & Environmental Science

ANALYSIS

View Article Online
View Journal | View Issue

Cite this: *Energy Environ. Sci.*, 2014, 7, 3459

Pathways to low-cost electrochemical energy storage: a comparison of aqueous and nonaqueous flow batteries†

Robert M. Darling,*[ab] Kevin G. Gallagher,*[ac] Jeffrey A. Kowalski,[ad] Seungbum Ha[ac] and Fikile R. Brushett[ad]

Received 11th July 2014
Accepted 12th September 2014

DOI: 10.1039/c4ee02158d

www.rsc.org/ees

Energy storage is increasingly seen as a valuable asset for electricity grids composed of high fractions of intermittent sources, such as wind power or, in developing economies, unreliable generation and transmission services. However, the potential of batteries to meet the stringent cost and durability requirements for grid applications is largely unquantified. We investigate electrochemical systems capable of economically storing energy for hours and present an analysis of the relationships among technological performance characteristics, component cost factors, and system price for established and conceptual aqueous and nonaqueous batteries. We identified potential advantages of nonaqueous flow batteries over those based on aqueous electrolytes; however, new challenging constraints burden the nonaqueous approach, including the solubility of the active material in the electrolyte. Requirements in harmony with economically effective energy storage are derived for aqueous and nonaqueous systems. The attributes of flow batteries are compared to those of aqueous and nonaqueous enclosed and hybrid (semi-flow) batteries. Flow batteries are a promising technology for reaching these challenging energy storage targets owing to their independent power and energy scaling, reliance on facile and reversible reactants, and potentially simpler manufacture as compared to established enclosed batteries such as lead–acid or lithium-ion.

Broader context

Cost-effective electrochemical energy storage has the potential to dramatically change how society generates and delivers electricity. A few key market opportunities include supporting high fractions of intermittent renewable energy sources and deferring upgrades of existing electricity grid infrastructure. Unfortunately, present state-of-the-art technologies are too expensive for broad deployment. Reductions in manufacturing costs and associated overheads are identified as the single largest cost-savings opportunity for today's battery-based storage options. In addition, increasing production volume and market competition will lead to lower material costs. Both aqueous and nonaqueous flow batteries are promising technology platforms capable of achieving the low costs required for widespread implementation. Non-aqueous systems enable higher cell voltages than their aqueous counterparts but also require higher active material solubility to offset higher electrolyte costs. For both battery types, a key enabling development will be the discovery of tailored molecules that are long lived, provide large cell voltages, and have costs similar to existing commodity chemicals.

1. Introduction

Energy storage is used to balance supply and demand on the electrical grid. The need to store energy is expected to increase as more electricity is generated from intermittent sources like wind and solar.[1–4] Pumped hydro installations currently account for greater than 95% of the stored energy in the United States, with a capacity equal to approximately 2.3% of generation.[5] Thermal storage, compressed air, flywheels, and batteries comprise the remaining 5% of storage capacity.[5] Other means of energy storage are also under investigation such as utilizing liquid fuels[6,7] (*e.g.*, H_2 or CH_4 generation and consumption) as well as utilization of existing resources[8] if a large electric vehicle fleet is established. The economics of storing grid energy is challenging. The Department of Energy's (DOE's) Advanced Research Projects Agency-Energy (ARPA-E) set a capital cost target of $100 per kW h for 1 hour of storage for widespread adoption.[9] The DOE Office of Electricity Delivery and Energy Reliability proposed cost targets of $250 per kW h by 2015, falling to $150 per kW h in the future for a fully integrated

[a]*Joint Center for Energy Storage Research,*
[b]*United Technologies Research Center, 411 Silver Lane, East Hartford, CT, 06108, USA. E-mail: darlinrm@utrc.utc.com*
[c]*Chemical Sciences and Engineering Division, Argonne National Laboratory, 9700 S Cass Avenue, Lemont, IL, 60439, USA. E-mail: kevin.gallagher@anl.gov*
[d]*Department of Chemical Engineering, Massachusetts Institute of Technology, 77 Massachusetts Avenue, Cambridge, MA, 02139, USA*

† Electronic supplementary information (ESI) available. See DOI: 10.1039/c4ee02158d

distributed energy storage system providing 4 h of storage.[10] The target cost of the energy storage device in the 2015 integrated system was $100 per kW h. These strict targets reflect the cheap cost of electricity in the United States. Fortunately, compared with transportation applications, batteries for grid applications can tolerate higher temperature and lower energy density; this widens the scope of possible solutions to include, for example, sodium–sulfur and redox flow batteries. Yang *et al.* recently reviewed electrochemical storage technologies for grid electricity.[11]

Comprehensive reviews of flow batteries include those of Weber *et al.*,[12] Ponce de Leon *et al.*,[13] and Skyllas-Kazacos *et al.*[14] The active species in most flow batteries are redox couples dissolved in liquid electrolytes that can be stored in inexpensive vessels, like plastic tanks. Fig. 1 schematically depicts a flow battery. The system includes electrochemical reactors, storage vessels, circulation pumps, a heat exchanger, and power conditioning equipment. The positive and negative electrolytes are fed to one or more electrochemical reactors, where the active species are oxidized or reduced to alternately charge or discharge the battery. Ideally, the redox reactions are facile, and the participation of solid components is limited to electron transfer, which is conducive to long cycle lives. Skyllas-Kazacos *et al.* report that durability generally exceeds 5000 deep cycles for flow batteries.[14] The energy densities of common aqueous flow systems, like vanadium redox (VRFB), are lower than those of enclosed batteries like lead–acid and lithium-ion (Li-ion). Fortunately, this deficiency can be tolerated in many stationary applications. Flow battery systems require pumps to circulate the electrolytes, resulting in parasitic losses and complicating independent operation on the grid.

Flow batteries are suited to storing megawatt-hours of electrical energy that is meant to be discharged over the course of hours. A compelling feature of flow batteries is the distinct separation of power and energy characteristics. The reactors and ancillary equipment are sized for power, while the amount of active material and volume of storage vessels are determined by energy. The cost of the battery asymptotically approaches the cost of the redox solutions at long discharge times (see Fig. 8 (ref. 15) for example). This clean division between power and energy is absent from conventional enclosed batteries. This decoupling may offer advantages in large installations because it alters the scaling of cost with energy. The cost of an electrochemical device generally scales with active area, while the cost of conventional chemical process equipment varies with volume raised to a power like 0.5–0.6.[16] The architecture of flow batteries suggests a mixed scaling. Reactor cost should scale with area, while the cost of the other components should scale similarly to traditional chemical process equipment. This benefit is somewhat muted at present by the high cost of the reactors relative to other major components.

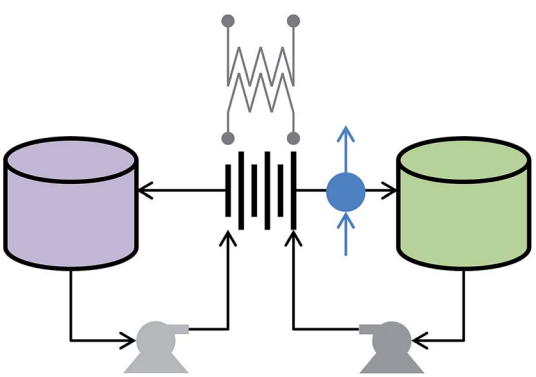

Fig. 1 Schematic diagram of a flow battery system.

The advent of modern redox flow batteries (RFBs) began with the development of the iron–chromium system at NASA in the 1970s.[12,17] Since then, a large number of aqueous RFBs have been developed including bromine–polysulfide, vanadium–polyhalide, and all-vanadium systems. In addition, several aqueous hybrid batteries have been pursued, where one or both electrode reactions are a deposition/dissolution process, such as zinc–bromine and soluble lead–acid systems. Though several of these technologies have been successfully demonstrated at large-scale, none have experienced widespread commercial success due to a number of technical and economic challenges. Though only sporadically investigated for the past 40 years, the renaissance of renewable electricity generators has spurred research and development in the field and led to a number of important recent advances including high performance electroreactors,[18–20] new electrolyte formulations,[21] and new tailored redox molecules.[22–24]

A recent area of research and development in the redox flow battery community is the identification, synthesis, and modification of novel redox active molecules.[6,12,23,25–37] These tailored molecules may be composed of organic constituents or ligand modified inorganic species. Tailoring molecules to have the necessary properties required of active species in redox flow batteries leverages the dramatic advances in synthetic chemistry made since the pioneering work on flow batteries in the 1970s and 1980s. Demonstrations with synthetic molecules have shown attractive cell voltages, fast kinetics, and low cost. The challenge in front of developers is to capture all of the aforementioned benefits in addition to high solubility, long cycle life, and low toxicity. While the majority of work to date has utilized aqueous electrolytes, nonaqueous electrolytes offer the attractive possibility of higher voltages.

As compared to their aqueous counterparts, non-aqueous redox flow batteries are in their infancy. In 1988, Matsuda *et al.* demonstrated the first non-aqueous redox flow battery based on a ruthenium bypyridine complex with an open circuit potential of 2.6 V.[38] Over the next few decades, non-aqueous electrolytes were sporadically investigated for redox flow batteries with the focus on anion-exchange systems which employ single electrolytes composed of metal coordination complexes.[27,28,31,37,39–41] Despite the promising cell potentials (>2 V), many of these systems have been hampered by limited solubility of the complexes, and low efficiencies. More recently, research efforts have broadened to include other redox materials most notably metal-centered ionic liquids[26] and tailored organic molecules[25,32] which have shown higher solubilities in non-aqueous electrolytes. A number of hybrid chemistries have also been

investigated, using lithium metal as an anode and a flowing positive electrolyte consisting of either polysulfides[42,43] or tailored molecules.[44] In general, most of these efforts have been exploratory with a focus on identifying new redox materials.

Transitioning from aqueous to nonaqueous electrolytes offers a wider window of electrochemical stability that enables operation at higher voltages.[25,45] Wang *et al.* illustrate the available voltage window and existing redox couples for aqueous electrolytes.[17] Depending on the salt, solvent, and electrode material, the stability window for nonaqueous electrolyte can span greater than 4 V.[46] High cell voltage leads to higher energy density, and typically to higher efficiency as well. These benefits promise to reduce the cost of energy. In addition, a greater selection of redox materials may be available due to either the wider potential window or the variety of available nonaqueous solvents.[25,47] Higher energy density also leads to smaller system footprint, which may enable specific applications like storage in an urban environment.[42,43] However, this promise must be balanced with the challenges associated with nonaqueous electrolytes, namely, increased cost, reduced ionic conductivity, and other unfavorable physical properties including moisture sensitivity, flammability, and toxicity. Furthermore, as compared to their aqueous counterparts, nonaqueous flow batteries are in their infancy, and many unknowns still exist. Understanding and balancing these competing factors will be key to determining the true prospects for nonaqueous flow batteries.

Cost estimates of various sophistication have been reported previously for aqueous flow batteries.[48–52] We seek to build upon the knowledge disseminated in those works and examine the technological potential of aqueous, and for the first time, nonaqueous flow batteries in achieving cost objectives. Our approach is to utilize the simplest model that maintains the essential performance and cost factors, enabling broad and meaningful discussions regarding material and system requirements. The analysis is intended to be flexible enough to facilitate comparison of different systems. Sources for performance and cost parameters are provided within the analysis where pertinent. Through a comparative analysis, we examine trends as well as areas of strength and future research needs. The exact values of system price presented here, which can be challenged on various grounds, are of secondary importance to our goals.

The goal of this paper is to examine the relationships among the cost and performance of the components and the final system price for flow batteries in a general way. This paper begins with a brief discussion of the economics of energy storage that provides an appreciation for the implications of price targets. This is followed by a mathematical description of the contributions to the price of a flow battery. The model is employed to determine sets of chemical and reactor costs, as well as area-specific resistance (ASR) and thermodynamic potential that yield a target battery price. These results are interpreted in the context of existing and conceptual aqueous and nonaqueous flow batteries. Solubility targets for the active species in nonaqueous batteries are derived from the chemical costs. Cost factors and ASR values for various battery systems are included to rationalize the range of parameters considered. Examples are shown that demonstrate how costs are predicted to fall between now and a future state in which 1% of all energy generated is stored in the battery under study. The future-state costs of enclosed, hybrid, and flow batteries are compared, so that the different technologies can be judged on equal footing. Finally, prospects for achieving necessary ASR and solubility values for conceptual aqueous and nonaqueous flow batteries are discussed with the aid of theoretical models and experimental data.

2. Economics of energy storage

A variety of techniques are available to evaluate the economic prospects of an engineering project. These include evaluations of discounted cash flow, net present worth, capitalized costs, payback time, and rate of return on initial investment. The first three methods account for the time value of money, while the last two do not, and are therefore less reliable. For the sake of simplicity, we assume continuous, uniform payments and continuous compounding in our analysis. Given these assumptions, the economics of the project can be described by a simple, first-order differential equation relating the principle, the net revenue stream, and the internal rate of return. Newman *et al.* presented an analysis of energy-storage systems subject to the above constraints and we follow their approach in this work.[53]

Newman *et al.* described the economics of energy storage with the equation:[53]

$$P_0 - N\frac{1-\exp(-rt_L)}{r} = 0 \quad (1)$$

where P_0 is the price of the installed energy storage system in dollars, N is the net revenue in \$ per year, t_L is the life of the battery in years, and r is an inflation-adjusted rate of return in per year. The variable r is often referred to as the "internal rate of return" (IRR). The ratio P_0/N is a simple payback time in years, and the factor $r/(1-\exp(-rt_L))$, referred to as the capital recovery factor for continuous payments and compounding, accounts for the time value of money. An IRR of 30% per year, which yields a payback time of 3.3 years in the limit of large t_L, is a reasonable benchmark for an industrial process with moderate technical risk.[16] An IRR of 10% per year is commonly used when establishing the economics of different energy storage scenarios.[1] Electric utilities often work with longer time horizons than other industrial and commercial concerns. Both battery price and net revenue can be normalized by the discharge energy of the battery to create intrinsic values.

The net revenue for a battery that stores energy purchased at a low price to be sold later at a higher price is given by:

$$N = (p_d E_d - p_c E_c)\omega = p_d E_d \omega\left(1 - \frac{p_c}{\varepsilon_{e,rt} p_d}\right) \quad (2)$$

The variable N is the net revenue in \$ per year, p is the price of electricity in \$ kW h^{-1} (or \$ J^{-1}), E is energy in kW h (or J), and ω is the frequency of deep cycling in per year. The subscript d denotes discharge, c denotes charge, and rt denotes round trip;

$\varepsilon_{e,rt}$ is the round trip energy efficiency of the battery system. Eqn (2) uses the energy discharged by the battery as a basis, while Newman *et al.* used charging energy.[53] This choice dictates where the energy efficiency appears in the equation, but is mathematically equivalent. The term in brackets on the right side of the equation indicates that the energy efficiency must exceed the ratio of electricity prices in order to achieve positive net revenue. Clearly, energy storage is most attractive when there is a large difference between peak and off-peak electricity prices. Excluded from our analysis are sources of revenue other than arbitrage, like managing demand charges, that may be available to batteries connected to the grid.

Eqn (1) and (2) may be combined to calculate how much storing energy in a battery adds to the cost of electricity:

$$p_d - p_c = \frac{P_0}{E_d \omega} \frac{r}{1 - \exp(-r t_L)} + p_c \left(\frac{1}{\varepsilon_{e,rt}} - 1 \right) \quad (3)$$

Casting the energy storage costs in this form was suggested by Poonpun and Jewell.[54] The cost added to the price of electricity, $p_d - p_c$, has the benefit that it is easily understood by all consumers who receive electric bills. The first term on the right shows that the price increase is proportional to the intrinsic capital cost of the battery, and inversely proportional to the cycling frequency. The second term on the right side of the equation shows how the cost and efficiency of charging affect the price increase. This term tends to be small because the factor in brackets tends to zero at high efficiency, and cheap electricity is typically used to charge the battery. For example, the final term is just \$0.0167 per kW h for p_c = \$0.05 per kW h and $\varepsilon_{e,rt}$ = 75%. This analysis does not contemplate battery replacements because flow batteries should be able to achieve the required number of cycles and longevity, as cited in the Introduction.

Fig. 2 shows the relationship between capital cost and the increase in electricity price for various internal rates of return. The electricity price increase at a particular capital cost rises with internal rate of return. For example, the electricity price increase at \$100 per kW h and 30% per year is identical to the price increase at \$200 per kW h and 10% per year. A storage device achieving a capital cost of \$100 per kW h would add \$0.08 per kW h to the electricity cost at an IRR of 10% per year. Average industrial and residential electricity rates in the United States were \$0.070 per kW h and \$0.118 per kW h in 2012, respectively.[55] Peak wholesale prices of approximately \$0.25 per kW h were observed in the Northeast and Mid-Atlantic regions of the United States in January 2014.[56] Electricity rates in many European countries and Japan are considerably higher than those in the United States,[55] making energy storage potentially more valuable in these markets. For example, industrial and residential rates in Japan were \$0.18 per kW h and \$0.26 per kW h in 2012.[55] Fig. 2 was drawn for ω = 250 per year, roughly equal to one cycle per weekday. Cycling daily or more frequently moderates the increase in electricity price associated with storage.

The simplicity and transparency of the preceding analysis help to clarify the cost of storage in arbitrage applications. More

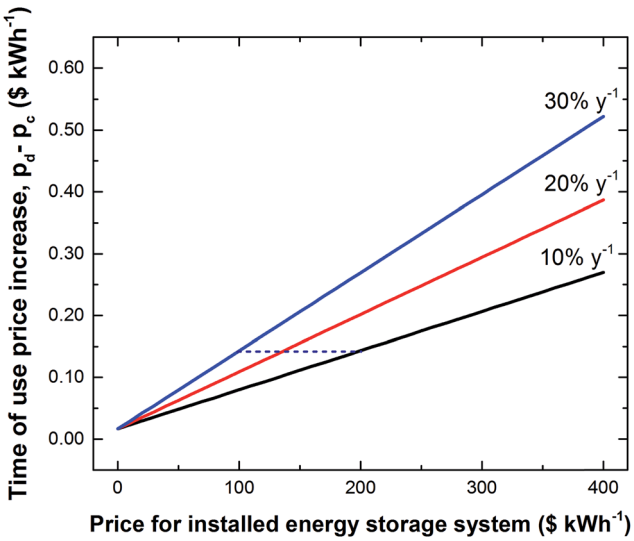

Fig. 2 Relationship between capital cost and electricity price increase for various internal rates of return. Calculations done with: $\varepsilon_{e,rt}$ = 75%, t_L = 10 years, ω = 250 per year, and p_c = \$0.05 per kW h. The dashed line illustrates the doubling of allowable capital costs when comparing a 10% per year return to a 30% per year at a price increase of \$0.14 per kW h.

comprehensive analyses of the markets for energy storage devices that include other applications and sources of revenue have been published. Sandia National Laboratories has reported discharge durations, addressable market sizes, and anticipated economic benefits for nineteen segments of the energy storage market.[57] The benefits are presented as present worths in units of \$ kW^{-1} based on 10 years of life at a discount rate of 10% with 2.5% escalation. Present worth in \$ kW^{-1} was converted to \$ per kW h by dividing by average discharge time. Reported values include \$245 per kW h for managing time-of-use energy costs and \$73 per kW h for managing demand charges. A flow battery could potentially accomplish both of these tasks for a building owner. Bundling services significantly reduces the cost barrier to market entry.

3. Mathematical description of capital cost

The price of a flow battery system can be apportioned into terms that scale with reactor area and electrolyte mass, as well as system costs that scale with power. Thus, the system price may be expressed as:

$$P_0 = c_a A + (c_{add} + c_{bop}) E_d t_d^{-1} + \sum_i c_{m,i} m_i \quad (4)$$

where P_0 is the initial system price in \$, c_a is the reactor cost per unit area in \$ m^{-2}, A is the electrode area in m^2, c_{bop} is the cost for balance-of-plant components in \$ kW^{-1}, c_{add} is the addition to the capital cost to reach the system price in \$ kW^{-1}, E_d is the energy discharged by the battery system in kW h (or J), t_d is the discharge time of the battery in h, $c_{m,i}$ is the cost per unit mass of electrolyte species i in \$ kg^{-1}, and m_i is the required mass of

species i in kg. Power conditioning equipment, controls, sensors, pumps, pipes, fans, filters, valves, and heat exchangers are included in c_{bop}. The cost of the electrolyte storage vessels is absorbed into the electrolyte mass term. The additional contribution to price, c_{add}, includes factors such as depreciation, labor, overhead, and margin. The assumptions behind these two parameters are detailed in the ESI.† Installation costs, which tend to be site and project specific and highly variable, are excluded from the price. We do not anticipate large differences in installation costs amongst different kinds of flow batteries. Aqueous systems will tend to be larger, while nonaqueous systems may require additional environmental controls. Sandia provides example installation costs for various battery systems.[1] Estimation methods based on multipliers established from a ratio of installation and service costs to the costs of purchased equipment are commonly used in the chemical processing industries. A flow battery resembles a small, simple chemical plant in many respects. Our cost analysis is limited to the price of the electrochemical reactors, the mechanical and electrical balance of plant, and the chemicals leaving the factory.

In our analysis, reactor area is determined by the discharging half cycle. The time available for charging is expected to exceed the discharge time in most applications, and thus discharging power density is the limiting attribute. Achieving high power density is typically easier on charge because the voltage is higher, even though the upper voltage is often limited to avoid deleterious side reactions. The area is determined by dividing the output power by the power density of the electrochemical reactor. These quantities are assumed to be constant during discharge for the sake of simplicity. Practically, the power density of the reactor will decline as the battery discharges, and the active species are consumed. System losses associated with auxiliaries that include electrolyte pumps and power conversion equipment force the electrochemical reactor to discharge more energy than appears in the external circuit. Accounting for these losses, the area of the electrochemical reactor can be calculated from the formula:

$$A = \frac{E_d}{\varepsilon_{sys,d} i_d V_d t_d} \tag{5}$$

where $\varepsilon_{sys,d}$ is an efficiency that accounts for losses associated with auxiliary equipment, including power conversion, electrolyte pumps, and heat exchanger fans, during discharge. The subscript d is needed because the efficiencies of the auxiliary equipment may differ on charge and discharge. The current density and voltage of the reactor are denoted i_d and V_d, respectively. Their product is the power density of the reactor in W cm^{-2} or kW m^{-2}. Pumping losses typically contribute less than 1% in a properly designed system.[18,51] However, the flowing electrolyte also takes the role of cooling the reactor. Other architectures without pumps will then be required to take on the burden of blowing cooled air or pumping a coolant. We choose to not distinguish between these burdens as they are a small portion of the total. Shunt currents that reflect the losses due to the required manifolds of flow batteries are reflected in the coulombic efficiency as presented below.

A key factor that distinguishes enclosed battery designs from those based on flow architectures is the relationship between power and energy. For flow batteries, the reactors may be independently sized to meet power and efficiency requirements regardless of the energy requirements. By contrast, stationary electrodes in enclosed and hybrid cells are commonly limited by transport within the electrode or other phenomena that scale with current density. For example, in hybrid cells that utilize a metal electrodeposition and dissolution reaction at the negative electrode, the current density is constrained below a maximum on charge to ensure that the desired plating morphology is obtained (*i.e.*, no dendrites). The reactor area is determined by either life or energy constraints rather than the target voltage efficiency. This typically results in larger reactors that are more expensive, albeit more efficient.

The round-trip energy efficiencies of the battery system and the electrochemical reactor are related by the equations:

$$\varepsilon_{rt} = \frac{E_d}{E_c} = \varepsilon_{sys,c}\varepsilon_{sys,d}\frac{E_{d,reactor}}{E_{c,reactor}} \tag{6}$$

where E_c and E_d are the charge and discharge energies of the battery system observed at the connection to the external power grid, and $E_{c,reactor}$ and $E_{d,reactor}$ are those energies observed at the electrical connections to the reactor. The energy ratios are round-trip energy efficiencies. In general, $\varepsilon_{sys,d}$ will depend on how the battery is operated. For example, pumping losses will increase with increasing flow through the system, and heat exchange losses will increase in proportion to ambient temperature in systems that require active cooling to maintain temperature below a prescribed maximum. Trading ε_{sys} with the efficiency of the reactor is an important aspect of design. For the simplified analysis presented in this paper, $\varepsilon_{sys,d}$ is treated as a constant.

The amounts of the electrochemically active species needed can be found by application of Faraday's law. Conservatively, the amount of electrolyte that must be stored in the system is determined by the charging requirements, since coulombic inefficiency results in $Q_d < Q_r < Q_c$, where Q is charge capacity in coulombs, and the subscripts d, r, and c denote discharge, reversible, and charge, respectively. The mass of the positive active material, for example, is given by:

$$m_+ = \frac{M_+ s_+ Q_c}{n_e F \chi} = \frac{M_+ s_+ Q_d}{\varepsilon_{q,rt} n_e F \chi} = \frac{M_+ s_+ E_d}{\varepsilon_{sys,d}\varepsilon_{q,rt} n_e F \chi V_d} \tag{7}$$

where m_+ is the mass of positive active species required to charge the battery, M_+ is the molecular weight, s_+ is the stoichiometry of the positive active species in the energy storage reaction, n_e is the number of electrons, F is the Faraday constant, and χ is the allowable state of charge (SOC) range. The SOC range is limited in order to avoid unwanted side reactions and disproportionately large flows in the system. With regard to flows, decreasing the minimum SOC from 20% to 10% requires a doubling of the pumping and plumbing capacities in order to maintain a constant stoichiometric excess. We replaced Q_c with Q_d in order to put all cost terms on the same basis. This change introduces the round-trip coulombic efficiency, $\varepsilon_{q,rt}$. Finally, the charge capacity was replaced with the ratio of energy to voltage.

This introduces the energy efficiency of the system, $\varepsilon_{sys,d}$, to account for losses associated with supporting equipment. Eqn (7) shows that the mass of electrolyte is inversely proportional to the discharge voltage. Thus, operating at low voltages is undesirable from the perspective of electrolyte cost.

The electrolyte is expected to make a significant contribution to the total cost of a nonaqueous flow battery. The electrolyte, in our terminology, includes a dissociated acid, base, or salt in a solvent, but excludes the active material. Explicitly accounting for the electrolytes and active species on the positive and negative sides yields:

$$\sum_i c_{m,i} m_i = \frac{E_d}{\varepsilon_{sys,d}\varepsilon_{q,rt} n_e F V_d}\left[\frac{s_+ M_+}{\chi_+}\left(c_{m,+} + \frac{c_{m,e+}}{S_+}\right) + \frac{s_- M_-}{\chi_-}\left(c_{m,-} + \frac{c_{m,e-}}{S_-}\right)\right] \quad (8)$$

The subscripts + and − denote the positive and negative active species, and the subscripts e+ and e− refer to the positive and negative electrolytes. S_+ is the solubility of the positive active species per unit mass of electrolyte in kg kg^{-1}. The solubility of a redox species is typically a function of oxidation state. The minimum of the solubilities for the oxidized and reduced forms should be used with enough margin to ensure that concentration polarization does not lead to deposits in the electrodes that hinder performance. A conflict between the solubilities of the salt and active species is likely to occur in practice. We chose not to distinguish the contributions of solvent and conductive species costs to limit the number of explicit parameters for ease of exposition. Expanding the expression for chemical costs to explicitly include the solvent and salt is straightforward, if justified.

A polarization equation relating i_d and V_d and relationships describing the system and coulombic efficiencies are needed to proceed with the analysis. A flow battery must operate efficiently, $\varepsilon_{e,rt} > p_c/p_d$, in arbitrage applications. It is, therefore, reasonable to expect a linear polarization response for a successful flow battery over the economically viable range of efficiencies:

$$V_d = U - i_d R \quad (9)$$

where the potential intercept, U, corresponds to the thermodynamically reversible or open-circuit potential, and R is the area-specific resistance (ASR) in Ω cm^2. The ASR includes ohmic losses in the bipolar plates and separator, as well as kinetic, ohmic, and transport losses in the electrodes. The potential intercept and the ASR generally depend on SOC. For example, the variation in U for a redox pair separated by one oxidation state that follows the Nernst equation is 113 mV between 10% and 90% SOC at 25 °C. The potential intercept and ASR are treated as constants in this work. Two important sources of coulombic inefficiency in flow batteries are crossover of active species through the membrane by diffusion and migration, and shunt currents in the manifolds connecting adjacent cells. The inefficiency caused by crossover decreases with increasing current density, while the inefficiency caused by shunt current decreases with decreasing voltage. Using thicker membranes will tend to reduce the crossover of active species at the expense of higher ASR. Using less conductive electrolytes will tend to reduce shunt currents. The effect on ASR is less straightforward in this case. The above mentioned effects are ignored in this work.

Combining expressions for reactor, electrolyte, and system costs and introducing the discharge voltage efficiency, $\varepsilon_{v,d} = V_d/U$, to simplify notation yields the following equation for the total system price for useable energy:

$$\frac{P_0}{E_d} = \frac{c_a R}{\varepsilon_{sys,d} U^2 \varepsilon_{v,d}(1-\varepsilon_{v,d}) t_d} + \frac{1}{\varepsilon_{sys,d}\varepsilon_{q,rt} n_e F \varepsilon_{v,d} U} \times \left[\frac{s_+ M_+}{\chi_+}\left(c_{m,+} + \frac{c_{m,e+}}{S_+}\right) + \frac{s_- M_-}{\chi_-}\left(c_{m,-} + \frac{c_{m,e-}}{S_-}\right)\right] + \frac{c_{add} + c_{bop}}{t_d} \quad (10)$$

The contribution of the reactor to the system cost is a minimum at $\varepsilon_{v,d} = 0.5$ and monotonically increases as $\varepsilon_{v,d}$ either increases or decreases according to eqn (10). Practically, the assumption of linear polarization will probably fail at low voltage efficiency as mass-transport effects become more important. The cost of the chemicals is a minimum at $\varepsilon_{v,d} = 1$ and increases monotonically with decreasing $\varepsilon_{v,d}$. There is a voltage efficiency that yields a minimum total price for any set of component cost and performance parameters, according to eqn (10). In the limit of long discharge times, the total system price approaches the chemical cost.

4. Results and discussion

4.1 Analysis of factors to achieve cost target

We are seeking to establish the performance and cost objectives necessary to achieve cost competitive energy storage for aqueous and nonaqueous flow batteries. While market opportunities currently exist at battery prices greater than $200 per kW h (see ref. 57 for example), we focus on aggressive targets that could enable dramatic penetration worldwide. First, we map a broad set of pathways to meet an aggressive metric of $120 per kW h for an energy storage system, not including installation costs. This value is in line with the rolled up installed capital cost target of $150 per kW h suggested by the U.S. DOE Office of Electricity Delivery and Energy Reliability.[5] Then we examine the likelihood of achieving the necessary technological and economic values. The areal costs for each flow battery include a flow field plate, an electrically insulating frame, a separator, seals, and two electrodes for each cell, and balance of stack materials such as end plates and tie rods. Component costs vary widely and depend on the materials used and the production volume considered. Table 1 lists the costs used in the analysis for 2014 and a mature, high-volume future state. To establish a frame of reference for "future state" cases, we calculate the annual production volume for flow batteries if used to store 1% of the electricity produced worldwide for five

Table 1 Component cost factors for flow batteries

Material	Year 2014 cost, \$ m^{-2}	Reference	Future state cost, \$ m^{-2}	Reference
Graphite flow field plate	55	51	25–35	51
Stainless-steel flow field plate	40	58 and 59	10–20	58 and 59
Carbon-fiber felt/paper electrodes	70	51	10–30	58 and 59
Fluorinated ion-exchange membrane	500	51	25–75	58–61
Polyolefin nanoporous separator	10	51	1–3	Est.
Fames, seals, and manifolds total	6	Est.	1–3	Est.

hours each day. In 2009, 20 000 TW h of electricity was produced worldwide.[4] Assuming daily use, 1% of electricity stored, and a 10 year battery life, ~10 GW h of new energy storage systems is required annually. This equates to 2 GW of power and thus $\sim 10^6$ m^2 of active area. For our calculations, values are taken from published literature on flow batteries and polymer electrolyte fuel cells where possible. Polymer electrolyte fuel cells and flow batteries share many design features and materials of construction. Fuel cells generally contain precious metal catalysts that are absent in flow batteries, conversely most fuel cells do not have insulating frames. The cost and performance characteristics of fuel cells have received considerable scrutiny because they are viewed as possible primary power sources for automobiles. When utilizing engineering estimates, we employed a comparison to similar high volume products and/or a bottom-up cost rationalization to determine long-run, high-volume costs.

The likelihood of achieving the low costs in the future state case is highly uncertain. We present the values here as one possible pathway to dramatically reduced energy storage costs that may be reached in the future. We note that both benefits from manufacturing scale and engineering advancements will likely be required to reach the optimistic values. However, we also note that the cited studies estimate even lower material costs for items like ion-exchange membranes and carbon-paper electrodes than the values used in this study when annual production volumes exceeding those considered in this analysis are reached.[58–60]

The analysis of the price of the battery system is presented in terms of the average chemical cost factor, c_m, needed to reach a system price of \$120 per kW h as a function of open-circuit potential, U, with the product c_aR as a parameter. The appearance of the product c_aR indicates that an expensive, high performance reactor and a cheap, low performance reactor may be equivalent in economic terms. The chemical cost factor is given by:

$$c_m = \frac{\varepsilon_{q,rt} n_e F U \chi}{2sM}\left[\varepsilon_{v,d}\varepsilon_{sys,d}\left(\frac{P_0}{E_d} - \frac{c_{add} + c_{bop}}{t_d}\right) - \frac{c_a R}{U^2(1-\varepsilon_{v,d})t_d}\right] \quad (11)$$

The positive and negative active species are assumed to be identical in terms of cost, molecular weight, ratio of s/n_e, and SOC range. The electrolyte cost factor, c_m, can be interpreted as the cost of the active material in a free electrolyte solution, or the cost of the combination of active material and electrolyte in a nonaqueous battery. Aqueous acidic solutions approach the ideal free electrolyte. For nonaqueous electrolytes, the solubility required to reach a given value of c_m can be calculated for prescribed values of $c_{m,+}$ and $c_{m,e+}$ from the equation:

$$c_m = c_{m,+} + \frac{c_{m,e+}}{S_+} \quad (12)$$

The subscripts + and − are interchangeable as we have assumed that the two electrolytes have identical properties. The contribution of the chemical costs was cast in the form of c_m to enable comparison with commodity chemical prices. However, we note that the quantity $sn_e^{-1}Mc_m$ which has units of \$ per mol e^- is a theoretically pleasing alternative that presents itself when examining eqn (10). The SOC range and coulombic efficiency could be included in this number to account for incomplete utilization of active material.

Table 2 summarizes the parameters used in the simulations presented in Fig. 3, where P_0/E_d is the target system price, \$120 per kW h, excluding installation. The discharge time of 5 h matches the average given by Sandia for time-of-use energy management.[57] The SOC range is typical of vanadium flow batteries. The coulombic efficiency, $\varepsilon_{q,rt}$, was set to 0.97 to capture both crossover and shunt current losses. The system efficiency was assumed to be $\varepsilon_{sys,d} = \varepsilon_{sys,c} = 0.94$. The voltage efficiency, $\varepsilon_{v,d} = 0.916$, was calculated to give $\varepsilon_{e,rt} = 0.75$, assuming that the magnitude of the discharging current density is twice that for charging. The corresponding voltage efficiency during charging is 0.96. The assumptions behind the balance-of-plant cost and additional contributions to price estimates are detailed in the supporting information. The oxidized and reduced forms of the active species were assumed to differ by one oxidation state. Species that can transfer more than one electron offer a considerable theoretical benefit. The assumed molecular weight of 0.1 kg mol^{-1} is a compromise that is higher than metals like Fe and V and lower than organic molecules like benzoquinone. A rough optimistic limit for organics is 1 electron equivalent per benzene ring, which yields an equivalent weight of $n_eM_i/s_i = 0.078$ g $(mol\ e^-)^{-1}$.

Fig. 3 illustrates lines of constant system price, \$120 per kW h, for the parameters in Table 2, and the combinations of c_aR listed in the figure. The abscissa is the open-circuit potential, U.

Table 2 Parameters used in system price calculations

P_0/E_d	t_d	χ	$\varepsilon_{sys,d}$	$\varepsilon_{q,rt}$	$\varepsilon_{v,d}$	$c_{add} + c_{bop}$	s/n_e	M
\$120 per kW h	5 h	0.8	0.94	0.97	0.916	\$300 per kW	1	100 g mol^{-1}

Aqueous batteries should be possible for $U < 1.5$ V. This exceeds the thermodynamic stability window of water in recognition of the fact that oxygen and hydrogen evolution are sluggish on carbon. Higher voltages likely require nonaqueous, aprotic electrolytes like those used in Li-ion batteries. Lead–acid and zinc–bromine batteries, with $U > 1.7$ V, are notable exceptions to this heuristic. The aqueous region is marked with two triangles in the lower left of the figure. The nonaqueous region is identified in a similar fashion, towards the upper right of the figure. The darkly shaded triangles are considered to have a higher likelihood of achievement compared to the larger and lightly shaded triangles. The left ordinate is the chemical cost factor, c_m, in \$ kg^{-1}. This cost factor is an average of the positive and negative sides and includes the active material, salt, solvent, and storage vessel costs on a mass of active material basis. The electrolyte should be inexpensive in the aqueous region; thus, c_m should correspond essentially to the sum of the active material and storage vessels only. A practical guideline for a minimum c_m for aqueous systems is \$2 kg^{-1}. Commodity prices will dictate the exact cost contribution, which will probably be higher (*e.g.*, vanadium costs \$23 kg^{-1}). The vertical scales inset on the left side of the figure aid in the interpretation of c_m for nonaqueous systems. The inner leftmost scale shows the solubility in kg kg^{-1} required to achieve a given chemical cost factor if active material and electrolyte cost \$5 kg^{-1} each. The rightmost scale converts the solubility to a concentration of active species, assuming specific volumes of 1 L kg^{-1}. The sloped, dashed lines represent different reactor costs, parameterized by the product c_aR. Table 4, to be discussed later, contains c_aR values that can be compared to the values in Fig. 3.

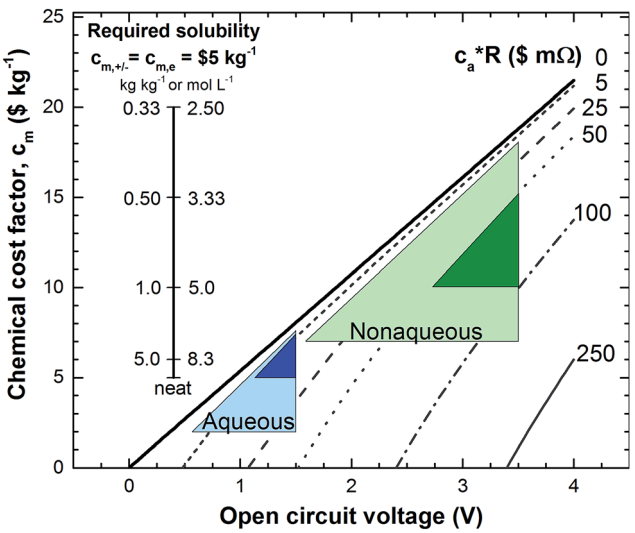

Fig. 3 Allowable chemical cost factor on an active material basis (in \$ kg^{-1}) *versus* open-circuit voltage for a range of reactor costs (c_aR in \$ mΩ). All points on a line give a system price of \$120 per kW h with the parameters given in Table 2. The region $U < 1.5$ V is considered to be available to aqueous systems. The dark shaded triangles are considered to have a higher likelihood of achievability compared to the larger lighter shaded triangles. The leftmost inset vertical scale shows the required solubility (in kg kg^{-1}) of a nonaqueous active species when solvent and solute cost \$5 kg^{-1}. The rightmost inset vertical scale on the right shows the molar concentration, assuming specific volumes of 1 L kg^{-1}.

The future cost of nonaqueous electrolytes and tailored molecules is difficult to forecast at the scale of a combined gigawatt hours of energy storage around the world. However, the commodity chemical industry provides some clues as to what a reasonable price for materials might be.[62,63] Annual production of a 3 V nonaqueous flow battery providing a combined 10 GW h of storage requires $\sim 10^4$ metric tons per year of electrolyte and active material and $\sim 10^6$ m^2 of membrane annually. Prices of commodities of similar or larger scale such as acetonitrile, propylene carbonate, triethylene glycol, and ethyl ether fall in the \$1–5 kg^{-1}.[62,64] Based on the trends observed for these, we selected \$5 kg^{-1} as a reasonable material price that could be achieved if volumes of electrolyte and active material on the order of 10^4 metric tons are demanded by the market. World-wide production of acetonitrile was near 10^5 metric tons in 2011, although only a portion of that amount was isolated and refined for resale.[62] An electrolyte includes both solvent and salt contributions, for which the salt is likely to be more expensive than the solvent, particularly if fluorinated and only used in a few industrial applications. The assumption of \$5 kg^{-1} for the electrolyte could be considered as \$2 kg^{-1} for the solvent and \$20 kg^{-1} for a salt at 1 M concentration; however, we lump the values together as a reflection of the inherent uncertainty contained in this analysis.

In Fig. 3, the top line, $c_aR = 0$, corresponds to a free reactor and gives the maximum possible chemical cost that yields the system price target of \$120 per kW h, subject to the parameters in Table 2, as a function of open-circuit voltage. This line prevails at long discharge times, as the contributions of the reactor and balance of plant diminish to zero. The lower lines correspond to higher reactor costs. The line at 5 \$ mΩ is consistent with an ASR of 0.5 Ω cm^2 and a reactor cost of \$100 m^{-2}. These values appear to be achievable with aqueous flow batteries having ion-exchange membranes and carbon bipolar plates for a high-volume, large-market future state. For the sake of comparison, ASR values as low 0.23 Ω cm^2 have been measured for H_2/Br flow batteries with thin membranes.[15] Elimination of the ion-exchange membrane in favor of a nanoporous separator, if technically palatable, would certainly reduce costs at lower production volumes. Nanoporous is taken

Table 3 Chemistry and design characteristics for candidate enclosed, flow, and hybrid architectures that are currently used and may be used in the future for energy storage. Performance values are for a 5 h discharge. A single solubility value, S, is used for both negative and positive electrolytes for simplicity[a]

Architecture		Enclosed	Enclosed	Flow	Flow	Flow	Hybrid	Hybrid	Hybrid
Chemistry		C-PbAcid PbC/PbO_2	Li-ion Gr/LFP	VRFB V^{2+}/V^{5+}	AqRFB TBD	NAqRFB TBD	Zinc Bromine Zn/Br_2	LiPS Li/Li_2S_8 (Li_4S_8)	NAqHyb Li/TBD
ASR, R	Ω cm^2	4.0	60.0	0.5	0.5	5.0	1.0	20.0	20.0
U	V	2.0	3.3	1.4	1.5	3.0	1.7	2.3	4.2
$\varepsilon_{v,d}$	—	0.98	0.99	0.92	0.92	0.92	0.98	0.95	0.97
$\varepsilon_{q,rt}$	—	0.90	1.00	0.97	0.97	0.97	0.90	0.95	0.95
Ψ_A	kW m^{-2}	0.22	0.01	2.84	3.25	1.30	0.62	0.12	0.23
χ_-	—	0.22	0.53	0.80	0.80	0.80	0.53	0.53	0.53
χ_+	—	0.16	0.80	0.80	0.80	0.80	0.80	0.80	0.80
S	kg kg^{-1}	7.8	3.8	0.1	0.2	1.0	0.2	1.0	1.0
s_-M_-/n_e	g (mol e$^-$)$^{-1}$	104	72	51	150	150	33	7	7
s_+M_+/n_e	g (mol e$^-$)$^{-1}$	120	158	51	150	150	194	135	150

[a] C-Pb/Acid = carbon-based advanced lead–acid, Gr/LFP = graphite/$LiFePO_4$ VRFB = vanadium redox flow battery AqRFB = aqueous redox flow battery NAqRFB = nonaqueous redox flow battery NAqHyb = nonaqueous hybrid LiPS = lithium polysulfide TBD = to be determined.

here to mean pore sizes less than 100 nm. Thus, an aqueous system meeting the \$120 per kW h target is possible with a chemistry that costs \$5 kg^{-1} and operates at 1.5 V. The line drawn for $c_aR = 50$ \$ mΩ represents a nonaqueous reactor cost of \$100 m^{-2} and ASR of 5 Ω cm.² The ASR is expected to be higher in nonaqueous batteries compared to aqueous electrolytes because of a lower electrolyte conductivity in the separator and within the electrodes. High-power Li-ion cells have pulse-power ASR >5 Ω cm^2 with more common values near 20 Ω cm^2.[65,66] Today's Li-ion batteries have area cost factors of approximately \$6 m^{-2} and potentially lowering to \$2–5 m^{-2} for higher volumes. This is at least a factor of 20 smaller than the optimistic future state area cost of flow batteries at \$100 m^{-2}. The larger voltage window of nonaqueous electrolytes allows for a wider range of c_aR values. As mentioned previously, power density scales with the square of voltage. In addition, stamped metal plates will likely replace the graphite flow fields, resulting in a net increase in c_aR over aqueous that is less than a factor of 10. The dark shaded region bounds the most likely set of parameters yielding a nonaqueous flow battery with a system price of \$120 per kW h. This region suggest $U > 3$ V and $S > 0.8$ kg kg^{-1} (a concentration of >4.4 mol L^{-1} with $M = 0.1$ kg mol^{-1} and a specific volume of 1 L kg^{-1}) with an active material that costs less than \$12 kg^{-1} and is compatible with an electrolyte costing \$5 kg^{-1}. These values are inexact, but they provide guidance regarding the combinations of potential, solubility, and performance that must be achieved in order to create a successful nonaqueous flow battery for storing grid energy. The quantities in Table 2 should be adjusted once a particular electrolyte and active material couple has been identified to improve accuracy.

Fig. 3 indicates that nonaqueous electrolytes enable a potentially wider range of cell voltages compared to aqueous electrolytes. Nonetheless, one must also consider two additional factors that potentially counteract this perceived advantage. First, the lead–acid battery teaches us that while the thermodynamic stability window of water is 1.2 V, a 2.0 V aqueous cell is possible when the kinetics of water splitting is slow. The products of water decomposition, H_2 and O_2, may be recombined advantageously to reform water. Energy storage systems based on enclosed architectures such as lead–acid and nickel–metal hydride are designed to promote this recombination.[67,68] An open architecture could also mitigate the loss of water by electrolysis with the addition of water to the reservoir, assuming that the gases escape from the system. Conversely, nonaqueous electrolytes generally undergo irreversible decomposition when pushed outside of their stability window, which results in various gas molecules, soluble compounds, and precipitants.[46,69] The precipitant is commonly associated with increased resistance to electron transport from the conducting surfaces (*i.e.*, passivity). If passivity is not achieved, the irreversible reaction will continue to consume the electrolyte, thereby dramatically increasing the battery impedance and shortening the useable life. The second consideration is the higher cost of nonaqueous compared to aqueous electrolytes. Current Li-ion electrolytes are reported to cost \$15–20 kg^{-1}, albeit at a relatively low production volume relative to commodity chemicals.[65,66] Conversely aqueous electrolytes cost significantly less than \$1 kg^{-1}.[70]

Fig. 4 illustrates the sensitivity of the required solubility to the cost and equivalent weight of the active material for an electrolyte that costs \$5 kg^{-1} and a battery price of \$120 per kW h. For low molecular weights and low active material costs, the required solubility is below 0.5 kg kg^{-1}. However, a solubility at or above 1 kg kg^{-1} is required for the target active material cost of \$5 kg^{-1} and a more reasonable equivalent weight of 100 g (mol e$^-$)$^{-1}$. The sensitivity to molecular weight raises an important issue related to the counter ion required by a tailored molecule. When a molecule undergoes a redox reaction, the newly formed charge is balanced with a cation or anion in the

electrolyte. If a molecule is transformed to a net positive valence, then an anionic counter ion is needed. In nonaqueous electrolytes, PF_6^- or BF_4^- might be considered as counter ions. Unfortunately, these fluorine-based anions are expensive constituents of current electrolytes. Additionally, the anions have large molecular weights and will quickly shrink the available design space to nothing. In contrast, aqueous systems may utilize inexpensive salts such as sulfur (*i.e.*, H_2SO_4). For aqueous electrolytes, an anion-paired tailored molecule would likely be reasonable. A commodity counter ion such as sulfur may also be possible in a nonaqueous battery, assuming a high enough conductivity is reached. However, cation-associating molecules are most likely to achieve the cost target.

4.2 Cost comparison of different battery technologies

Table 3 shows performance characteristics for various battery chemistries using enclosed, flow, or hybrid architectures. Mature conventional batteries, both aqueous and nonaqueous, are included together with various existing and conceptual flow batteries. These values are combined with the cost factors in Table 4 to estimate representative system prices for 2014 and prices for a potential future state, excluding installation. This future state is an example of one possible pathway to cost-effective storage that may be reached through high-volume production, market competition, and engineering advances. Table 3 also includes reported prices for battery chemistries that are available for grid integration today. The performance and cost values are taken from the literature, private discussions with industry experts, and engineering estimates. The ESI† contains details regarding the calculation for each battery chemistry considered. The majority of the 2014 prices are taken from the EPRI/DOE handbook,[1] which compiled surveys for megawatt-scale energy storage devices from industrial suppliers.

Examination of the power density, Ψ_A, reported in Table 3 illustrates that nonaqueous batteries can approach similar power densities to aqueous batteries. Greater differences are seen across different battery architectures than within a single class. The vanadium redox flow battery (VRFB), future-state tailored-molecule aqueous redox flow battery (AqRFB), and future-state tailored-molecule nonaqueous redox flow battery (NAqRFB) are projected to exhibit power densities on the order of >1 kW m^{-2} for a continuous 5 h discharge at 75% round-trip efficiency. While nonaqueous electrolytes commonly have lower conductivity and thus higher ASR, a nonaqueous electrolyte can support higher cell voltages. Reactor cost is proportional to c_a, R, and U^{-2}. Thus, if the potential is increased from 1.5 to 3 V, the product c_aR can increase by a factor of 4 without causing the cost of the reactor to increase. Recently, Aziz *et al.* demonstrated a tailored quinone in an aqueous electrolyte that had an ASR on par with VRFB and the values assumed for AqRFB.[23] A more detailed evaluation of ASR and power density is provided later in this paper.

The area of a flow reactor is sized specifically for a target discharge efficiency. However, enclosed batteries are commonly limited by other factors such as mass transport or decay mechanisms that result in the comparatively low power densities for the graphite/$LiFePO_4$ (Gr/LFP) battery and carbon-based advanced lead–acid (C-PbAcid) battery. The electrode capacity densities used here are 2 mA h cm^{-2} for Gr/LFP and 60 mA h cm^{-2} for C-PbAcid. If Gr/LFP were not limited to a maximum electrode thickness of 100 μm, then a target discharge voltage efficiency of 91.6% would result in electrodes 3-fold thicker and power density a factor of 10 higher. The power density that is measured during a 5 h discharge is not representative of pulse power capability, which can be much higher. The power densities of enclosed batteries during pulses that are seconds in duration far exceed the values in Table 3. More discussion on the limitations of enclosed cells may be found in the ESI.†

Hybrid architectures that utilize a metal negative electrode and a fluid reactant at the positive electrode capture some of the benefits of flow batteries, but are still constrained by a stationary electrode. The hybrid designs in Tables 3 and 4 are limited by the maximum allowable current density for the metal electrode considered. The current density constraint for metal electrodes is set by the need to control morphology during plating, when the battery is charging.[71,72] Assuming that the time available for charging is twice that for discharging, then the magnitude of the discharge current is approximately double the maximum charging current. The charge limitation is taken to be 20 mA cm^{-2} for zinc and 3 mA cm^{-2} for lithium. Lithium metal cycles poorly above 1.5 mA cm^{-2} as a result of poor lithium plating morphology control and irreversible capacity loss.[73] Crowther and West have visualized lithium dendrite growth at a current density of 2 mA cm^{-2}.[74] Thus, 3 mA cm^{-2} represents a dramatic advance in the ability to control lithium metal plating morphology, perhaps through a convection mediated approach.[72] A sensitivity analysis is presented in the ESI† highlighting the importance of improving charge acceptance if lithium metal is to be used in a hybrid battery.

Fig. 5 illustrates the existing cost structure and potential future states for the Gr/LFP based Li-ion enclosed battery as well as the VRFB. The system price is separated into four

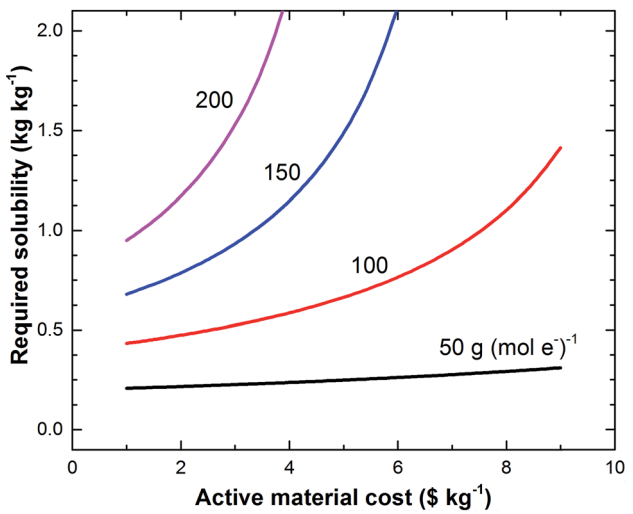

Fig. 4 Solubility requirements for a nonaqueous redox flow battery. Lines of constant equivalent weight are shown.

Table 4 Cost factors for enclosed, flow, and hybrid architectures that are currently used and may be used in the future for energy storage. The cost factors for 2014 assumed in this analysis are detailed in the ESI. Additionally, the lower and upper 95% confidence intervals (L95% and U95%, respectively) for projected future states of each technology are also listed

	C-PbAcid PbC/PbO_2	Li-ion Gr/LFP	VRFB V^{2+}/V^{5+}	AqRFB TBD	NAqRFB TBD	Zinc Bromine Zn/Br_2	LiPS Li/Li_2S_8 (Li_4S_8)	NAqHyb Li/TBD
Negative $c_{m,-}$ \$ kg^{-1}								
Est. 2014	5	18	29	20	20	2	200	200
Future L95%	3	9	7	3	3	1	60	60
Future U95%	5	15	37	7	7	2	140	140
Positive $c_{m,+}$ \$ kg^{-1}								
Est. 2014	3	15	29	20	20	15	10	20
Future L95%	2	8	7	3	3	3	1	3
Future U95%	3	12	37	7	7	10	3	7
Electrolyte $c_{m,e}$ \$ kg^{-1}								
Est. 2014	0.1	15	0.1	0.1	15	0.2	15	15
Future L95%	0.1	5	0.1	0.1	3	0.1	3	3
Future U95%	0.1	15	0.1	0.1	7	0.2	7	7
Area c_a \$ m^{-2}								
Est. 2014	20	6	700	700	700	205	100	100
Future L95%	17	2	70	70	55	45	10	10
Future U95%	20	5	175	175	160	105	50	50
Addition to price c_{add} \$ kW^{-1}								
Est. 2014	1250	1100	1550	1550	1550	500	1550	1550
Future L95%	150	250	50	50	75	50	75	75
Future U95%	250	350	125	125	150	125	150	150
BOP c_{bop} \$ kW^{-1}								
Est. 2014	350	550	410	410	410	410	360	360
Future L95%	105	200	145	145	145	145	115	115
Future U95%	220	325	260	260	260	260	230	230
System price P_o/E_d \$ per kW h								
Reported min	438	500	572	N/A	N/A	337	N/A	N/A
Est. 2014 min	443	509	564	664	695	355	685	565
Future L95%	155	193	118	106	114	103	119	93
Future U95%	196	254	207	148	156	160	195	140
Areal cost factor, c_aR in \$ mΩ (for comparison with Fig. 3)								
Est. 2014 min	10	45	44	44	438	26	250	250
Future L95%	9	15	4	4	34	6	25	25
Future U95%	10	38	11	11	100	13	125	125

contributions. The reduction in each of these factors between the reported 2014 minimum price and the projected future state price is shown in Fig. 5. Descriptions of these contributions, sources of information, and assumptions are documented in the ESI.† The energy and power costs are related to materials costs, with the quantities determined by the performance of the chemistry and the cell. The balance-of-plant cost, c_{bop}, captures system complexity through purchased items such as heating and cooling equipment, state-of-charge management, power electronics, and pumps if required. The costs of the storage vessels are added to the electrolyte and active materials, because these three costs should scale together with energy. The additional contribution to price, c_{add}, captures the manufacturing cost, sales, general costs, administration costs, research and development costs, and profit quantities necessary to mark up the materials cost to a system price. The 2014 c_{add} estimates were found by subtracting the material and purchased items costs from battery prices reported in the literature, after correcting for any installation costs.

The largest decrease in total system price for Li-ion batteries and VRFBs is the result of smaller c_{add} values. The 10 GW h production scale considered in this analysis has the potential to enable this dramatic cost reduction.[65,75,76] Established large-format Li-ion factories are commonly on the order of 1 GW h in annual production.[77] The C-PbAcid batteries are also projected to benefit from a larger scale in recognition that current production levels are not at the volumes enjoyed by automotive starting lighting and ignition or forklift batteries.[78] The projected C-PbAcid battery prices approach those commonly reported for valve-regulated lead–acid batteries, but with

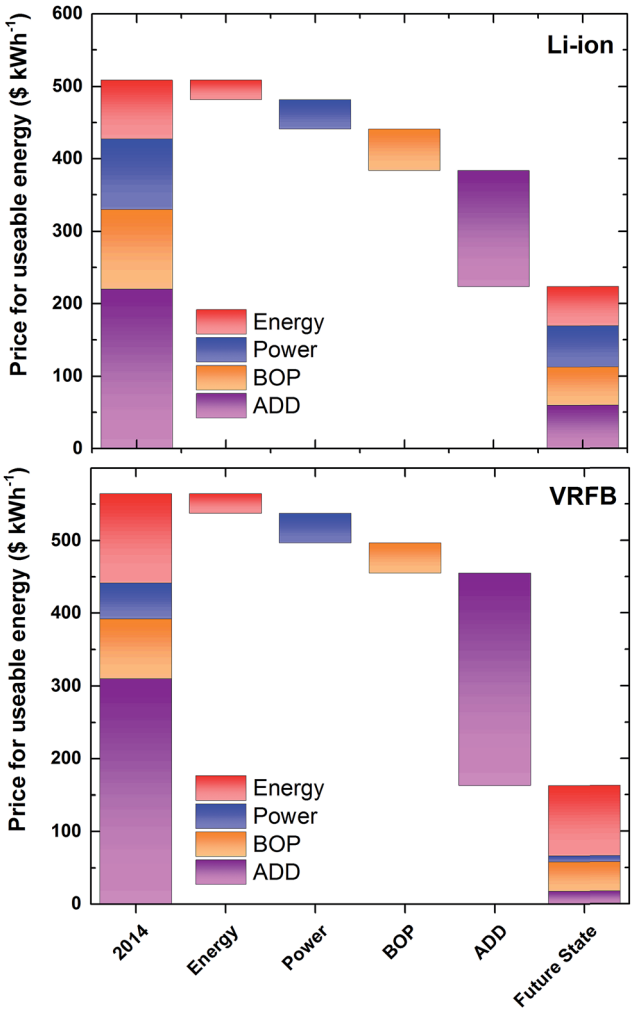

Fig. 5 Waterfall plots for Gr/LFP-based Li-ion (top) and VRFB (bottom) illustrating a potential pathway to reach cost effective energy storage. Here, balance of plant (BOP) is equivalent to c_{bop} on an energy basis. In both cases, the largest decrease occurs in the additional contributions to price factor (ADD) that encompasses depreciation, overhead, labor, *etc.*

potentially longer cycle life.[68,78] In Table 4 and Fig. 5, the future values of c_{bop} and c_{add} are highly uncertain, but are included in an attempt to close the gap between material costs and the total equipment cost realized by the owner of the energy storage system. More importantly, these values demonstrate the dramatic lowering of price contributions that must occur to reach long-term goals. Competitive pressures, benefits from scale, and benefits from learning by doing will all be driving forces for these projected cost reductions. Whether or not the assumed values are reached depends on both the existence of a profitable energy storage market that utilizes the chemistry in question and the quality of the engineering estimates.

For the high volume competitive market place projections, VRFB is shown to have significantly smaller additional contributions to price than Li-ion or C-PbAcid. This projected future state is based on the assumption that flow batteries require a comparatively simpler assembly process than enclosed batteries. This is supported by the direct comparison of the US Department of Energy funded manufacturing cost models for Li-ion and fuel cells.[58,59,65] The future state manufacturing cost calculations made for the assembly of proton exchange fuel cells were examined to estimate values for the additional contributions to the price factor of flow batteries.[58,59] The 2 GW annual production volume based capital depreciation and labor costs for pressing, slitting, assembling, sealing, and conditioning the reactor were less than \$6 kW^{-1}, after the lower power density for the flow battery (*i.e.*, 10 *vs.* 2 kW m^{-2}) had been taken into consideration (details in ESI†).[44,45] We note the power density of an automotive fuel cell is rated at a considerably lower efficiency than a flow battery is. The report did not provide the required mark-up values on depreciation and labor necessary to reach a full system price and thus we estimated these multipliers here using the same framework as the BatPaC Li-ion model. Based on this minimal manufacturing cost contribution, we use a future-state value for additional contribution to price that ranges from \$50 to \$125 kW^{-1} (details in ESI†). Nonaqueous flow batteries are charged an additional \$25 kW^{-1} in recognition of higher likelihood of complexity in the assembly process (*e.g.*, need for a dry room). Future work will examine in greater detail the manufacturing cost and additional mark-up of a flow-battery assembly process.

Fig. 6 illustrates the range of projected future-state battery prices compiled from the values in Tables 3 and 4. Uncertainty was calculated through a Monte-Carlo analysis to capture the upper and lower 95% confidence interval for each battery chemistry. Uncertainty was only considered for cost inputs. The cost breakdown for the mean battery price value is shown to illustrate the relative contributions of each component. However, the range of uncertainty is most instructive when

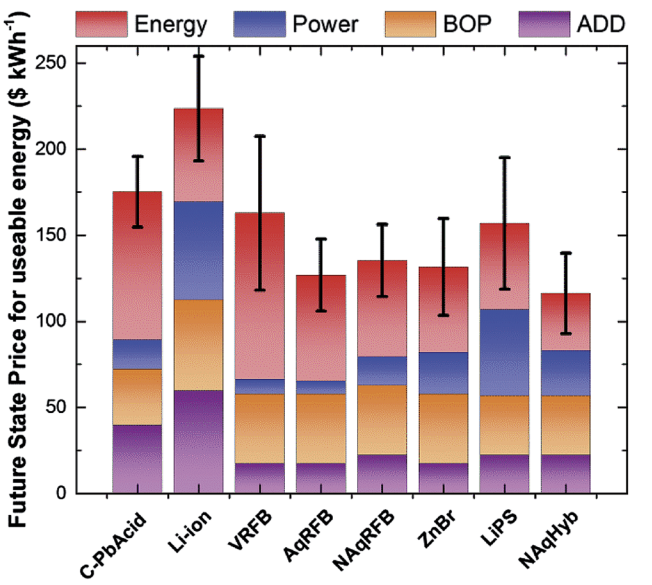

Fig. 6 Projected future state system prices for a range of different battery chemistries and architectures. The flow battery architectures have the lowest comparative values resulting from lower costs for power (reactor costs) and lower additional contributions (ADD) to price derived from an anticipated lower cost of manufacture. Here, balance of plant (BOP) is equivalent to c_{bop} on an energy basis.

comparing different batteries. Some batteries have significant uncertainty owing to commodity fluctuations, such as the vanadium in the VRFB. This projection does not take into account any resource recovery and recycling that may be possible. Other batteries, such as lithium polysulfide (LiPS), exhibit significant uncertainty as a result of calculated design and resulting sensitivity to a wide range in areal material cost factors. The LiPS battery has a modest average open circuit voltage of 2.25 V and is limited to relatively small charging current densities. In contrast, a battery design that combines a nonaqueous tailored molecule with lithium metal (NAqHyb) has nearly twice the voltage of LiPS and the same charging current limitation. The NAqHyb is much less sensitive to the wide range in area cost factors, and its higher power density results in a lower cost of power. The lithium metal batteries were both designed with a porous separator rather than a more costly ion-exchange membrane. However, the greater power density of the full flow architecture results in an overall lower cost of power.

As shown in Fig. 6, batteries utilizing closed architectures (C-PbAcid and Gr/LFP) are projected to be more expensive than those based on flow architectures. This difference in system price results from the lower reactor cost associated with the flow architecture, and from the lower additional contributions to price factor. The presumed simpler assembly process for a flow battery is projected to be a key distinguishing factor compared to enclosed cells. An additional discriminator, not captured in our economic analysis, is the reliance of flow batteries on facile reactions. These reactions are expected to be less susceptible to degradation than those that occur at stationary electrodes in enclosed cells like lead acid and involve more active participation of solid materials that can cause fatigue. Li-ion chemistries that undergo sizable volume expansion are also prone to cycle-based degradation. However, most Li-ion chemistries experience minimal volume expansion. The limiting factor for cells with graphite anodes is the growth of the solid-electrolyte interphase through electrolyte decomposition and, with it, the irreversible consumption of cyclable lithium. It is unknown at this time if nonaqueous flow batteries will age in a manner more similar to aqueous flow batteries or enclosed Li-ion cells. For nonaqueous hybrid approaches, significant advances are required to enable lithium metal-based systems to reach life goals in excess of 5000 cycles with minimal capacity loss.

In the comparative analysis of Fig. 6, little difference is seen between AqRFB and NAqRFB. Nonaqueous approaches do not seem to provide a step change in opportunity beyond aqueous approaches. The differentiation between these two electrolyte platforms must fall to the chemists and engineers that will develop the tailored molecules and systems that store them. Nonaqueous electrolytes inherently offer a wider range of possibilities to explore beyond aqueous systems. However, the new constraints of solubility and electrolyte (solvent + salt) cost in the nonaqueous medium may be more constrictive than the promise of a larger design space.

The VRFB and AqRFB have nearly identical power, balance of plant, and additional costs. The energy cost is lower for the AqRFB, however the difference is much less than one might anticipate based on the prices of the active materials. While vanadium costs approximately 4× more than the tailored organic molecule in \$ kg^{-1}, the equivalent weight of the organic molecule in g $(mol\ e^{-})^{-1}$ is approximately 3× more than vanadium. Achieving a low equivalent weight with an organic molecule is likely to be challenging.

4.3 Properties of aqueous and nonaqueous flow batteries

To assess the likelihood of achieving the estimated performances and costs, we compare key measured physical, transport, and kinetic properties of aqueous and nonaqueous electrolytes. Fig. 7 shows properties for a number of nonaqueous electrolytes. The properties have been normalized by dividing by the quantity appropriate for the VO^{2+}/VO_2^{+} positive electrode couple of a VRFB; the separator is assumed to be a Nafion ion-exchange membrane. The ESI† contains additional information about the electrolytes that is not included in the figure. The selected properties are pertinent to kinetic, ohmic, and mass transport losses in the electrochemical reactor as well as pumping losses and, indirectly, electrolyte cost. The arrows indicate better properties. Nonaqueous electrolytes have conductivities approximately two orders of magnitude lower than aqueous electrolytes. This difference drives comparatively higher ASR, although the additional losses may be less than proportional because, in cell designs without a gap, the ohmic losses associated with the electrolyte occur in a porous electrode that, in many designs, contains a highly conductive solid phase. This aspect will be discussed in more detail in the subsequent section on modeling. The second column in Fig. 7 shows the relative conductivity of the separator between the electrodes. The separators include Nafion exposed to different organic electrolytes, which give conductivities differing by an order of

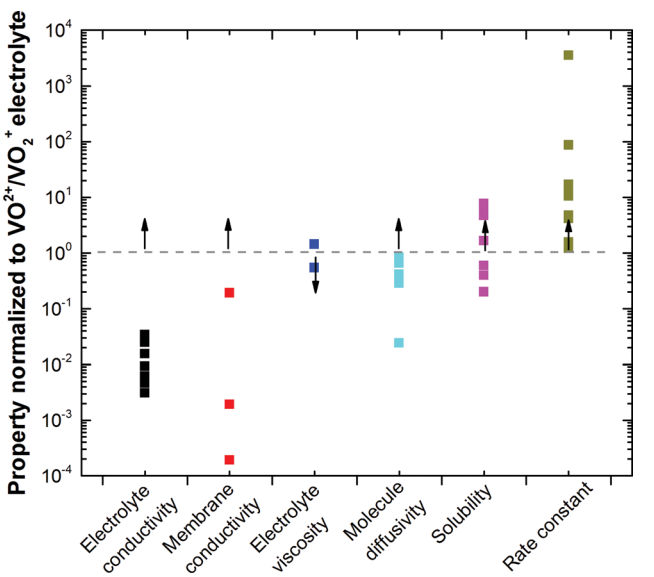

Fig. 7 Physical properties of select nonaqueous electrolytes normalized by the quantity describing the VO^{2+}/VO_2^{+} couple of a VRFB. A Nafion membrane is assumed for VRFB. The arrows indicate the direction of better nonaqueous properties.

magnitude, and ceramic electrolytes. The ohmic loss through the separator makes a proportional contribution to ASR; therefore, this difference between aqueous and nonaqueous batteries is particularly important. Whether or not an ion-exchange membrane is required in either an aqueous or nonaqueous system with two flowing electrolytes is an open question. Clearly, minimizing transport of active species across the separator is desirable in order to maintain high coulombic efficiency and to eliminate the need for separation processes. However, a combination of tailored active species and membranes with low hydraulic conductivity may possibly satisfy these requirements for either aqueous or nonaqueous systems. For reference, a lithium battery electrolyte in a polypropylene separator has conductivity near the maximum shown in Fig. 7.

As shown in the third column of Fig. 7, nonaqueous viscosities range near aqueous values, indicating that it should be possible to achieve similar pumping losses. Nonaqueous active species tend to have lower diffusion coefficients than metal ions like vanadium. The higher mass transport losses may not be important because nonaqueous cells will tend to operate at lower current densities than aqueous cells because of ohmic losses. Transport losses can usually be addressed by increasing intra-electrode velocity, at the expense of higher pumping losses. The solubility of a nonaqueous active species must be high because the supporting electrolyte is relatively expensive. The data in column 5 indicate that high solubility is possible in some nonaqueous systems. The final column indicates that high rate constants can be achieved in nonaqueous systems. The importance of this result is shown in the subsequent modeling section.

4.4 Modeling of ASR

The probability of future nonaqueous and aqueous flow batteries attaining low reactor cost is a direct function of the range of achievable ASR values. We employed a mathematical model based on porous-electrode theory to determine physically realistic ASR values. The model treats polarization losses in the direction perpendicular to the plane of the membrane. The electrode thickness is optimized to achieve the smallest ASR while maintaining the target discharge voltage efficiency of 91.6%. Liquid electrolyte is continuously forced through the electrodes in a primary flow direction that is parallel to the membrane. The electrodes are assumed to be inert, porous carbon felts or papers. This is a common electrode structure for aqueous flow batteries.

The cell potential may be expressed as:

$$V = (\Phi_{1,+} - \Phi_{1,-}) = (\Phi_{1,+} - \Phi_{2,+}) - (\Phi_{1,-} - \Phi_{2,-}) - \Delta\Phi_{\text{ohm}} \quad (13)$$

The first and second terms in the final equality signify the potential drops across the positive and negative electrodes. The final term captures ohmic losses in the membrane, current collectors, and contact resistances. The subscripts 1 and 2 denote the solid and electrolyte phases; the subscripts + and − denote the positive and negative electrodes. Analytical solutions are available for the potential drop across a porous electrode when either linear or Tafel kinetics applies, in the absence of mass-transport limitations.[79–81] The linear solution was used for $i < ai_0L$; the Tafel expression was used otherwise. The ASR was calculated by dividing $(U - V_d)$ by i_d. By this definition, ASR is not necessarily a local tangent to the polarization curve. The ASR is independent of current density when the linear approximation applies to the electrodes.

Properties that affect the voltage drop across a porous electrode include thickness L, electrolyte conductivity κ, solid conductivity σ, interfacial area per unit volume a, exchange current density i_0, anodic transfer coefficient α_a, and cathodic transfer coefficient α_c. The conductivities are corrected for the porosity and tortuosity of the electrode. Interfacial area per unit volume can be calculated from the fiber diameter (assuming high aspect ratio) and porosity. The exchange current density is related to the rate constant by Faraday's law. Both transfer coefficients were assumed to be 0.5 following convention in the absence of more detailed information.[82] The reader is referred to the aforementioned literature for complete descriptions of the potential drops across porous electrodes in the linear and Tafel regimes. Given the wide range of reaction rate constants in the literature, we have chosen to present results in terms of ASR *versus* rate constant, with optimistic values for other parameters.

Table 5 contains parameters, aside from rate constants, used in the simulations. Simulations were conducted for aqueous and nonaqueous cells with either Nafion or an inert nanoporous separator. The properties of the solid matrix were identical for all simulations. The electrode porosity, fiber diameter, solid conductivity, and contact resistance were measured for a moderately compressed carbon paper.[18] Bulk electrolyte conductivities include 229 mS cm^{-1} for an aqueous solution of 1.5 M VO^{2+} in 4.0 M total sulfate,[83] 52 mS cm^{-1} for Nafion in contact with the same solution,[84] and 5 mS cm^{-1} for 1 M $LiPF_6$ in propylene carbonate,[69] and less than 1 mS cm^{-1} for Nafion in contact with lithium salts dissolved in aprotic solvents.[85,86] Conductivity in the nanoporous separators is the bulk electrolyte conductivity corrected with the Bruggeman correlation for a porosity of 50%, raised to power of 1.5. The solid conductivity is considerably higher than either the aqueous or nonaqueous electrolyte conductivity.

Fig. 8 shows the calculated ASR as a function of kinetic rate constant for hypothetical aqueous and nonaqueous cells. The ASR is calculated at a discharge voltage efficiency of 91.6%. The electrode thickness is optimized to give the minimum ASR at the target efficiency for each rate constant, subject to a minimum of 50 μm and a maximum of 5000 μm, respectively. A more conservative minimum is 100 μm when pressure drop from convective flow is considered. The ratio of nonaqueous-to-aqueous power densities is shown in Fig. S3 in the ESI† assuming 3 V and 1.5 V, respectively. The resistance is between 0.5 and 30 times higher for the nonaqueous cell in the range of rate constants examined, with the largest differences occurring for large kinetic rate constants. The difference in limiting ASR at high rate constants is driven by the membrane resistivity for nonaqueous compared to aqueous conditions. While this is not

Table 5 Parameters used in electrode simulations

	Aqueous		Nonaqueous	
Parameter	Nanoporous separator	Nafion	Nanoporous separator	Nafion
Electrode porosity	0.81			
Fiber diameter (μm)	7.7			
Solid conductivity (mS cm^{-1})	3600			
Contact resistance (Ω cm^2)	0.068			
Reactant concentration (mol L^{-1})	2			
Membrane thickness (μm)	50			
Bulk electrolyte conductivity (mS cm^{-1})	229	229	5	5
Membrane conductivity (mS cm^{-1})	109	52	2	1
Membrane resistance (mΩ cm^2)	46	96	2507	5014

a direct function of the bulk electrolyte conductivity, the chemical physics driving the differences is likely similar.

Cation mobility in an electrolyte is related to multiple phenomena, but the most important in this comparison are likely the mode of conduction, solvated radius, and the solvent viscosity.[69] Aqueous electrolytes that conduct protons or hydroxide ions as the primary charge carrier benefit from the Grotthuss hopping mechanism, which utilizes the hydrogen bonding network present in water. The transport of other ions in aqueous and nonaqueous electrolytes is governed by diffusion in an electric field, a markedly slower process. Examination of the Stokes–Einstein equation shows that the diffusivity is inversely proportional to solvent viscosity and solvated ion radius.[69] In general, the solvated radius of aqueous electrolytes is smaller than nonaqueous electrolytes, leading to expectations of faster conduction in aqueous electrolytes in line with experimental observations. Ion transport in nanoporous separators is expected to be directly proportional to the bulk electrolyte. In the case of cation-selective membranes, such as Nafion, while the Grotthuss mechanism still enables proton hopping, the transport of other ions is impacted by the cation type, the solvent choice, and the dissociation of the cation from the fixed anion site (anion basicity).[85,86] Doyle and co-workers showed that ionic conductivities for the N117 (Li^+) membrane exceed 10^{-3} S cm^{-1} at room temperature for a number of nonaqueous solvents.[86]

Solid lines in Fig. 8 represent the improvement in ASR if a 50 μm-thick nanoporous separator replaces Nafion. The nonaqueous ASR is significantly reduced by this change. Conversely, a separator of 100 μm thickness would result in the same ASR and perhaps a more acceptable crossover contribution to the coulombic inefficiency. The higher voltage that is achievable in nonaqueous electrolytes can counterbalance a higher ASR, resulting in acceptable reactor power density (power density is proportional to U^2R^{-1}). The key factors in determining the relative comparison are the rate constant and the conductivity of the membrane. Fig. 8 and S5† support the selection of ASR values used in Table 3 and demonstrates that nonaqueous chemistries should be able to achieve adequate power densities. While this analysis was completed for room temperature, operating at higher temperatures is an alternative pathway to reducing the ASR and thus system cost.

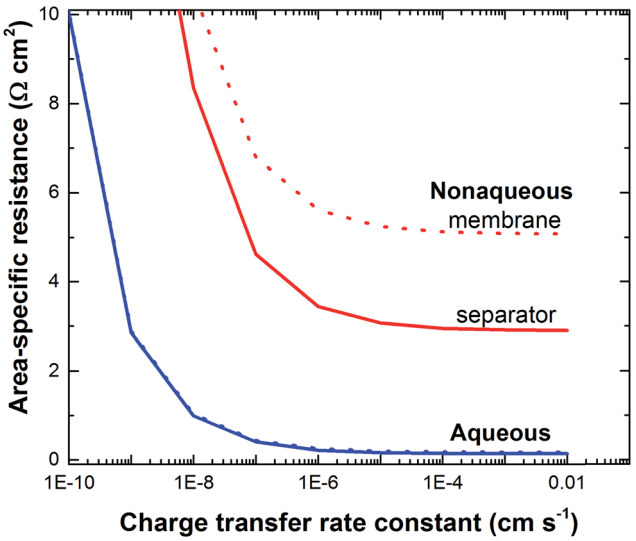

Fig. 8 Simulation of area-specific resistance for nonaqueous and aqueous cells. The solid lines correspond to a 50 μm Nafion membrane; the dashed lines correspond to a 50 μm nanoporous separator.

4.5 Membrane *vs.* porous separator

Recently, the development of aqueous redox flow batteries has benefitted tremendously from parallel efforts in fuel cells. In comparison, nonaqueous redox flow batteries are still in their infancy, and the extent to which the acquired knowledge from fuel cell and Li-ion battery development can be applied remains to be seen.

Presently, although Nafion is expensive, it is the preferred membrane for most aqueous redox flow batteries due to its high proton conductivity and chemical stability. Dramatic reductions in cost can be expected with increased manufacturing volumes (*i.e.*, over an order of magnitude[58–60]). Recent research efforts have primarily focused on optimizing existing Nafion membranes, through chemical and physical modifications, for specific redox flow battery chemistries or exploring potentially less expensive alternative membranes. Schwenzer *et al.*

Table 6 Performance and cost parameters required to meet cost effective energy storage

	U_{ave}, V	ASR, Ω cm^2	Equivalent weight, g (mol e−)$^{-1}$	Solubility mass basis, kg kg^{-1}	Solubility molar basis, mol L^{-1}	Material c_m, \$ kg^{-1}	Electrolyte c_e, \$ kg^{-1}
Nonaqueous	3	5	150	0.8	~4–5	5	5
Aqueous	1.5	0.5	150	0.05	~1–2	5	0.1

comprehensively reviewed the current state of membrane development for vanadium redox flow batteries, highlighting efforts in cation-exchange fluorocarbon, cation-exchange hydrocarbon, anion-exchange and amphoteric polymers, and nonionic separators.[87,88] The key challenge for these alternative membranes is maintaining or improving upon the ionic conductivity, selectivity, and chemical stability of Nafion without increasing the manufacturing costs. Replacing ion-conducting membranes with porous separators could lead to immediate cost reductions, provided the reactor design could be modified to account for the likely increase in crossover of active species.

Significantly less is known about the development needs of nonaqueous membranes beyond ionic conductivity. Of particular interest for flow batteries is the chemical stability to redox electrolytes, physical stability in large format cell, and species selectivity. The present state of membrane development for nonaqueous redox flow batteries was recently reviewed by Shin *et al.*[34] Their report highlighted that anion-exchange membranes are employed in the majority of nonaqueous cells primarily due to the chemistries under investigation (*i.e.*, metal-centered coordination complexes). While few cell chemistries employ cation-exchange membranes, this number is expected to increase due to the diversity of potential redox materials and the need to increase energy density. A body of literature exists for cation-exchange polymeric and ceramic solid electrolytes for rechargeable Li-ion and Li-metal batteries.[85,86,89] Indeed, several materials deemed unsuccessful for these applications (*e.g.*, unstable against Li metal) may find utility for nonaqueous redox flow batteries. Under nonaqueous conditions, replacing ion-selective membranes with porous separators could lead to cost reductions and appreciable improvements in ASR, provided the reactor design is modified to account for the likely increase in crossover. Although significant improvement is possible in the science and engineering of nonaqueous ion conductors, they will not surpass aqueous proton (or hydroxide)-based conductors with regard to conductivity.

5. Conclusions and path forward

Materials-level performance and cost requirements are presented in Table 6. Both aqueous and nonaqueous electrolyte platforms would benefit from tailored molecules with low equivalent weights, fast kinetics, and cell voltages that stretch the electrolyte stability window. The active material and electrolytes must both be inexpensive. Nonaqueous electrolytes should be no greater than \$5 kg^{-1}, and aqueous electrolytes must be almost free. Targets for the concentrations of active materials are 5 mol L^{-1} and 2 mol L^{-1} for nonaqueous and aqueous systems, respectively. Finally, the sensitivity of the nonaqueous system to salt cost and the equivalent weight of the active material suggests that successfully tailored molecules will utilize cation-based counter ions.

Nonaqueous flow batteries are far from a commercial reality at the time of this publication. This analysis provides the first quantitative guidance for researchers to consider in their exploration of chemical systems that, through maturation, may provide cost-effective energy storage. Unlike aqueous flow batteries, an archetype nonaqueous redox couple is not yet established. Examples of intriguing pathways for nonaqueous redox electrolytes that are aligned with the above goals could follow disparate routes. Reducing the unneeded molecular complexity of known redox structures to minimize equivalent weight (*e.g.*, modifying Li-ion overcharge protection molecules) can reduce cost and may lead to increased charge carrier concentration. Conversely, suspensions of electroactive polymers with multiple redox moieties can be created to achieve required charge carrier concentration and potentially obviate the need for an ion exchange membrane.

Both aqueous and nonaqueous flow batteries have pathways to reach long-term objectives for cost-effective energy storage. The design space for nonaqueous appears to be broader than that of aqueous systems. However, the constraints for nonaqueous systems of active material solubility and electrolyte cost create additional hurdles that must be overcome before a system of technological interest can be developed. Additionally, lower risk existing technologies that require less development like C-PbAcid, Li-ion, and VRFB will reach cost effective system price levels for many applications if large enough production volumes are demanded by the marketplace.

Nomenclature

a	Interfacial area per unit volume, cm^{-1}
A	Electrode area, m^2
c	Cost factor, use specific units
E_c	Energy to charge battery, kW h
E_d	Energy to discharge battery, kW h
F	Faraday constant, C (mol e$^-$)$^{-1}$
i	Current density, A cm^{-2}
i_0	Exchange current density, A cm^{-2}
L	Thickness, cm
M	Molecular weight, kg mol^{-1}
n	Number
N	Net revenue, \$ per year

p	Electricity price, $ per kW h
P_0	System price, $
Q	Charge, C
r	Internal rate of return, per year
R	Area-specific resistance, Ω cm^2
R	Universal gas constant, J mol^{-1} K^{-1}
s	Stoichiometric coefficient
S	Solubility, kg kg^{-1}
t	Time, h or year
T	Temperature, C or K
U	Potential intercept, V
V	Voltage, V

Greek symbols

α_a	Anodic transfer coefficient
α_c	Cathodic transfer coefficient
χ	State-of-charge
ε	Efficiency
κ	Electrolyte conductivity, S cm^{-1}
ν^2	Dimensionless exchange current density
σ	Solid conductivity, S cm^{-1}
Ψ_A	Power density, kW m^{-2}
ω	Deep discharge cycles, per year

Subscripts

a	Area
add	Additional contributions to price
bop	Balance of plant
c	Charge
d	Discharge
e	Electrolyte
i	Species i
L	Life
m	Material
q	Coulombic
rt	Round trip
sys	System
v	Voltage
+	Positive electrolyte
−	Negative electrolyte

Abbreviations

AqRFB	Aqueous redox flow battery
ARPA-E	Advanced Research Projects Agency-Energy
ASR	Area-specific resistance
C-PbAcid	Carbon-based lead-acid
DOE	Department of Energy
Gr/LFP	Graphite/$LiFePO_4$
IRR	Internal rate of return, per year
LiPS	Lithium polysulfide
NAqHyb	Nonaqueous hybrid redox flow battery
NAqRFB	Nonaqueous redox flow battery
SOC	State-of-charge
TBD	To be determined
VRFB	Vanadium redox flow battery

Acknowledgements

This work was supported as part of the Joint Center for Energy Storage Research, an Energy Innovation Hub funded by the U.S. Department of Energy, Office of Science, Basic Energy Sciences. The submitted manuscript has been created by UChicago Argonne, LLC, Operator of Argonne National Laboratory ("Argonne"). Argonne, a U.S. Department of Energy Office of Science laboratory, is operated under Contract no. DE-AC02-06CH11357.

References

1 A. A. Akhil, G. Huff, A. B. Currier, B. C. Kaun, D. M. Rastler, S. B. Chen, A. L. Cotter, D. T. Bradshaw and W. D. Gauntlett, *DOE/EPRI 2013 Electricity Storage Handbook in Collaboration with NRECA*, Sandia National Laboratories, Albuquerque, New Mexico 87185 and Livermore, California 94550, 2013.
2 M. Carbajales-Dale, C. J. Barnhart and S. M. Benson, *Energy Environ. Sci.*, 2014, **7**, 1538–1544.
3 *Medium-Term Renewable Energy Market Report 2013*, Paris, 2013.
4 S. Chu and A. Majumdar, *Nature*, 2012, **488**, 294–303.
5 I. Gyuk, M. Johnson, J. Vetrano, K. Lynn, W. Parks, R. Handa, L. Kannberg, S. Hearne, K. Waldrip, R. Braccio, *Grid Energy Storage*, Washington D.C., 2013.
6 U. Eberle, B. Mueller and R. von Helmolt, *Energy Environ. Sci.*, 2012, **5**, 8780–8798.
7 U. Eberle and R. von Helmolt, *Energy Environ. Sci.*, 2010, **3**, 689–699.
8 W. Kempton and J. Tomic, *J. Power Sources*, 2005, **144**, 280–294.
9 *Grid-Scale Rampable Intermittent Dispatchable Storage ARPA-E Funding Opportunity Announcement*, Washington D.C., 2010.
10 D. Rastler, *Market Driven Distributed Energy Storage System Requirements for Load Management Applications*, Electric Power Research Institute, Palo Alto, CA, 2007.
11 Z. Yang, J. Zhang, M. C. W. Kintner-Meyer, X. Lu, D. Choi, J. P. Lemmon and J. Liu, *Chem. Rev.*, 2011, **111**, 3577–3613.
12 A. Z. Weber, M. M. Mench, J. P. Meyers, P. N. Ross, J. T. Gostick and Q. Liu, *J. Appl. Electrochem.*, 2011, **41**, 1137–1164.
13 C. P. de Leon, A. Frias-Ferrer, J. Gonzalez-Garcia, D. A. Szanto and F. C. Walsh, *J. Power Sources*, 2006, **160**, 716–732.
14 M. Skyllas-Kazacos, M. H. Chakrabarti, S. A. Hajimolana, F. S. Mjalli and M. Saleem, *J. Electrochem. Soc.*, 2011, **158**, R55–R79.
15 C. Kyu Taek, P. Albertus, V. Battaglia, A. Kojic, V. Srinivasan and A. Z. Weber, *Energy Technol.*, 2013, **1**, 596–608.

16 M. S. Peters and K. D. Timmerhaus, *Plant design and economics for chemical engineers*, McGraw-Hill, New York, 4th edn, 1991.
17 W. Wang, Q. Luo, B. Li, X. Wei, L. Li and Z. Yang, *Adv. Funct. Mater.*, 2013, **23**, 970–986.
18 R. M. Darling and M. L. Perry, *J. Electrochem. Soc.*, 2014, **161**, A1–A7.
19 D. S. Aaron, Q. Liu, Z. Tang, G. M. Grim, A. B. Papandrew, A. Turhan, T. A. Zawodzinski and M. M. Mench, *J. Power Sources*, 2012, **206**, 450–453.
20 Q. H. Liu, G. M. Grim, A. B. Papandrew, A. Turhan, T. A. Zawodzinski and M. M. Mench, *J. Electrochem. Soc.*, 2012, **159**, A1246–A1252.
21 L. Li, S. Kim, W. Wang, M. Vijayakumar, Z. Nie, B. Chen, J. Zhang, G. Xia, J. Hu, G. Graff, J. Liu and Z. Yang, *Adv. Energy Mater.*, 2011, **1**, 394–400.
22 B. Huskinson, S. Nawar, M. R. Gerhardt and M. Aziz,in *Stationary and Large Scale Electrical Energy Storage 2*, ed. J. Meyers, J. Fenton, C. P. DeLeon, J. Weidner and T. VanNguyen, 2013, vol. 53, pp. 101–105.
23 B. Huskinson, M. P. Marshak, C. Suh, S. Er, M. R. Gerhardt, C. J. Galvin, X. Chen, A. Aspuru-Guzik, R. G. Gordon and M. J. Aziz, *Nature*, 2014, **505**, 195–198.
24 B. Yang, L. Hoober-Burkhardt, F. Wang, G. K. S. Prakash and S. R. Narayanan, *J. Electrochem. Soc.*, 2014, **161**, A1371–A1380.
25 F. R. Brushett, J. T. Vaughey and A. N. Jansen, *Adv. Energy Mater.*, 2012, **2**, 1390–1396.
26 P. J. Cappillino, H. D. Pratt, III, N. S. Hudak, N. C. Tomson, T. M. Anderson and M. R. Anstey, *Adv. Energy Mater.*, 2014, **4**, 1300566.
27 M. H. Chakrabarti, R. A. W. Dryfe and E. P. L. Roberts, *Electrochim. Acta*, 2007, **52**, 2189–2195.
28 M. Junyoung, L. Myung-Jin, P. Joung-Won, O. Duk-Jin, L. Doo-Yeon and D. Seok-Gwang, *Electrochem. Solid-State Lett.*, 2012, **15**, A80–A82.
29 W. Wang, W. Xu, L. Cosimbescu, D. Choi, L. Li and Z. Yang, *Chem. Commun.*, 2012, **48**, 6669–6671.
30 Y. Xu, Y.-H. Wen, J. Cheng, G.-P. Cao and Y.-S. Yang, *Electrochim. Acta*, 2010, **55**, 715–720.
31 T. Yamamura, Y. Shiokawa, H. Yamana and H. Moriyama, *Electrochim. Acta*, 2002, **48**, 43–50.
32 L. Zhen, L. Sha, L. Suqin, H. Kelong, F. Dong, W. Fengchao and P. Sui, *Electrochem. Solid-State Lett.*, 2011, **14**, A171–A173.
33 D. Amadeo, *et al.*, Electrochemical Energy Storage Systems and Methods Featuring large Negative Half-Cell Potentials, WO 2014/019605 A1, 2014.
34 S.-H. Shin, S.-H. Yun and S.-H. Moon, *RSC Adv.*, 2013, **3**, 9095–9116.
35 Z. Song and H. Zhou, *Energy Environ. Sci.*, 2013, **6**, 2280–2301.
36 D. Lloyd, T. Vainikka, M. Ronkainen and K. Kontturi, *Electrochim. Acta*, 2013, **109**, 843–851.
37 Q. Liu, A. A. Shinkle, Y. Li, C. W. Monroe, L. T. Thompson and A. E. S. Sleightholme, *Electrochem. Commun.*, 2010, **12**, 1634–1637.
38 Y. Matsuda, K. Tanaka, M. Okada, Y. Takasu, M. Morita and T. Matsumurainoue, *J. Appl. Electrochem.*, 1988, **18**, 909–914.
39 M. H. Chakrabarti, E. P. L. Roberts, C. Bae and M. Saleem, *Energy Convers. Manage.*, 2011, **52**, 2501–2508.
40 Q. Liu, A. E. S. Sleightholme, A. A. Shinkle, Y. Li and L. T. Thompson, *Electrochem. Commun.*, 2009, **11**, 2312–2315.
41 A. E. S. Sleightholme, A. A. Shinkle, Q. Liu, Y. Li, C. W. Monroe and L. T. Thompson, *J. Power Sources*, 2011, **196**, 5742–5745.
42 Y. Yang, G. Zheng and Y. Cui, *Energy Environ. Sci.*, 2013, **6**, 1552–1558.
43 F. Y. Fan, W. H. Woodford, Z. Li, N. Baram, K. C. Smith, A. Helal, G. H. McKinley, W. C. Carter and Y.-M. Chiang, *Nano Lett.*, 2014, **14**, 2210–2218.
44 X. Wei, L. Cosimbescu, W. Xu, J. Hu, M. Vijayakumar, J. Feng, M. Y. Hu, X. Deng, J. Xiao, J. Liu, V. Sprenkle and W. Wang, *Adv. Energy Mater.*, 2014.
45 M. Duduta, B. Ho, V. C. Wood, P. Limthongkul, V. E. Brunini, W. C. Carter and Y.-M. Chiang, *Adv. Energy Mater.*, 2011, **1**, 511–516.
46 K. Xu, *Chem. Rev.*, 2004, **104**, 4303–4417.
47 L. Su, E. Carino and F. Brushett, Massachusetts Institute of Technology, Cambridge, MA USA, unpublished work.
48 G. Hall and K. Michaels, *Cost Projections for Redox Energy Storage Systems*, United Technologies Corporation, 1980.
49 J. A. Mellentine, *Performance Characterization and Cost Assessment of an Iron Hybrid Flow Battery*, University of Tennessee, 2011.
50 Z. Mengqi, M. Moore, J. S. Watson, T. A. Zawodzinski and R. M. Counce, *J. Electrochem. Soc.*, 2012, **159**, A1183–A1188.
51 V. Viswanathan, A. Crawford, D. Stephenson, S. Kim, W. Wang, B. Li, G. Coffey, E. Thomsen, G. Graff, P. Balducci, M. Kintner-Meyer and V. Sprenkle, *J. Power Sources*, 2014, **247**, 1040–1051.
52 L. Joerissen, J. Garche, C. Fabjan and G. Tomazic, *J. Power Sources*, 2004, **127**, 98–104.
53 J. Newman, P. G. Hoertz, C. A. Bonino and J. A. Trainham, *J. Electrochem. Soc.*, 2012, **159**, A1722–A1729.
54 P. Poonpun and W. T. Jewell, *IEEE Trans. Power Appar. Syst.*, 2008, **23**, 529–534.
55 *Key World Statistics*, International Energy Agency, 2012.
56 http://www.eia.gov/todayinenergy/detail.cfm?id=14671, accessed June 26, 2014.
57 J. Eyer and G. Corey, *Energy Storage for the Electricity Grid: Benefits and Market Potential Assessment Guide*, Sandia National Laboratories, Albuquerque, New Mexico 87185 and Livermore, California 94550, 2010.
58 B. D. James, J. A. Kalinoski and K. N. Baum, *Mass Production Cost Estimation of Direct H2 PEM Fuel Cell Systems for Transportation Applications: 2010 Update*, Directed Technologies, Inc, Arlington, VA, 2010.
59 B. D. James and A. B. Spisak, *Mass Production Cost Estimation of Direct H2 PEM Fuel Cell Systems for Transportation Applications: 2012 Update*, Strategic Analysis Inc, Arlington, VA, 2012.

60 M. F. Mathias, R. Makharia, H. A. Gasteiger, J. J. Conley, T. J. Fuller, C. J. Gittleman, S. S. Kocha, D. P. Miller, C. K. Mittelsteadt, X. Tao, S. G. Yan and P. T. Yu, *Electrochem. Soc. Interface*, 2005, **14**, 24–35.
61 S. Eckroad, *Vanadium Redox Flow Batteries: An In-Depth Analysis*, Electric Power Research Institute, Palo Alto, CA, 2007.
62 *Chemical Economics Handbook*, IHS Chemical, 2011.
63 J. Anderson, *Chem. Eng. Prog.*, 2009, **105**, 27–31.
64 *Propylene Carbonate (PC) (CAS 108-32-7): Market Research Report 2013*, Business Analytic Center, 2013.
65 P. Nelson, K. Gallagher, I. Bloom and D. Dees, *Modeling the Performance and Cost of Lithium-Ion Batteries for Electric Vehicles*, Chemical Sciences and Engineering Division, Argonne National Laboratory, ANL-11/32, Argonne, IL USA, 2011.
66 P. A. Nelson, K. G. Gallagher and I. Bloom, *BatPaC (Battery Performance and Cost) Software*, http://www.cse.anl.gov/BatPaC/, 2012.
67 M. Fetcenko, in *Handbook of Batteries*, ed. D. Linden and T. B. Reddy, McGraw-Hill, New York, 3rd edn, 1995, ch. 30, pp. 30.31–30.37.
68 A. J. Salkind, R. O. Hammel, A. G. Cannone and F. A. Trumbore, in *Handbook of Batteries*, ed. D. Linden and T. B. Reddy, McGraw-Hill, New York, 3rd edn, 1995, ch. 24, pp. 24.21–24.46.
69 *Nonaqueous Electrochemistry*, ed. D. Aurbach, CRC Press, 1999.
70 M. Anderman, F. R. Kalhammer and D. MacArthur, *Advanced Batteries for Electric Vehicles: An Assessment of Performance, Cost, and Availability*, The Year 2000 Battery Technology Advisory Panel prepared for the California Air Resources Board, Sacramento, CA 2000.
71 P. c. Butler, P. A. Eidler, P. G. Grimes, S. E. Klassen and R. C. MIles, in *Handbook of Batteries*, ed. D. Linden and T. B. Reddy, McGraw-Hill, New York, 3rd edn, 1995, ch. 39, pp. 39.31–39.22.
72 R. D. Naybour, *J. Electrochem. Soc.*, 1969, **116**, 520–524.
73 D. Aurbach, E. Zinigrad, H. Teller and P. Dan, *J. Electrochem. Soc.*, 2000, **147**, 1274–1279.
74 O. Crowther and A. C. West, *J. Electrochem. Soc.*, 2008, **155**, A806–A811.
75 Gigafactory, http://www.teslamotors.com/sites/default/files/blog_attachments/gigafactory.pdf, accessed June 26, 2014, 2014.
76 K. G. Gallagher, S. Goebel, T. Greszler, M. Mathias, W. Oelerich, D. Eroglu and V. Srinivasan, *Energy Environ. Sci.*, 2014, **7**, 1555–1563.
77 C. Pillot, *The worldwide battery market 2011–2025*, Batteries 2012, Nice, France, 2012.
78 D. A. J. Rand and P. T. Moseley, in *Electrochemical Energy Storage for Renewable Sources and Grid Balancing*, ed. P. T. Moseley and J. Garche, Newnes, Oxford, 2014, ch. 13, p. 360.
79 J. Newman and K. E. Thomas-Alyea, *Electrochemical Systems*, Wiley Interscience, New York, 3rd edn, 2004.
80 J. S. Newman and C. W. Tobias, *J. Electrochem. Soc.*, 1962, **109**, 1183–1191.
81 J. Euler and W. Nonnemacher, *Electrochim. Acta*, 1960, 269–286.
82 A. J. Bard and L. R. Faulkner, *Electrochemical methods: fundamentals and applications*, John Wiley & Sons, Inc, 2nd edn, 2001.
83 M. Skyllas-Kazacos and M. Kazacos, *J. Power Sources*, 2011, **196**, 8822–8827.
84 Z. Tang, R. E. Keith, D. S. Aaron, J. S. Lawton, A. B. Papandrew and T. A. Zawodzinski, in *Large Scale Energy Storage for Smart Grid Applications*, ed. R. Savinell, J. Meyers, S. R. Narayan and D. Wheeler, 2012, vol. 41, pp. 25–34.
85 M. Doyle, M. E. Lewittes, M. G. Roelofs and S. A. Perusich, *J. Phys. Chem. B*, 2001, **105**, 9387–9394.
86 M. Doyle, M. E. Lewittes, M. G. Roelofs, S. A. Perusich and R. E. Lowrey, *J. Membr. Sci.*, 2001, **184**, 257–273.
87 B. Schwenzer, J. Zhang, S. Kim, L. Li, J. Liu and Z. Yang, *ChemSusChem*, 2011, **4**, 1388–1406.
88 X. Li, H. Zhang, Z. Mai, H. Zhang and I. Vankelecom, *Energy Environ. Sci.*, 2011, **4**, 1147–1160.
89 J. W. Fergus, *J. Power Sources*, 2010, **195**, 4554–4569.